Semi-fluorinated Surfactant Syntheses of Ordered Porous Materials with Tailorable Pore Sizes

Xiangju Meng, Yan Di, Lan Zhao, Dazhen Jiang, Shougui Li, and Feng-Shou Xiao*

Department of Chemistry & State Key Laboratory of Inorganic Synthesis and Preparative Chemistry, Jilin University, Changchun 130012, P. R. China

Received February 18, 2004. Revised Manuscript Received August 13, 2004

Novel ordered mesoporous silica-based materials (JLU-14 and JLU-15) with tailorable size are successfully synthesized by changing crystallization temperatures in both strongly acidic media and neutral conditions using semi-fluorinated surfactant [FSO-100, $CF_3(CF_2)_4$-$(EO)_{10}$] as a template. JLU-14 and JLU-15 show much higher hydrothermal and mechanical stability than those of MCM-41, which are assigned to their relatively thicker mesoporous walls. Characterization of samples by X-ray diffraction (XRD), transmission electron microscopy (TEM), and N_2 adsorption shows that the pore sizes of JLU-14 and JLU-15 are estimated to vary from micropore to mesopore (1.6−4.0 nm) with various crystallization temperatures (room temperature to 100 °C). Furthermore, heteroatoms such as Ti species are effectively introduced into mesoporous silica of JLU-14 from various routes, and catalytic data show that Ti−JLU-14 assembled from preformed TS-1 nanoclusters is very active. Moreover, the semi-fluorinated surfactant syntheses are not limited to the use of FSO-100, and many semi-fluorinated surfactants are candidates only if they can effectively form regular micelles in solution. Therefore, semi-fluorinated surfactant synthesis is a new route to prepare a series of stable ordered mesoporous silica and heteroatom-incorporated silica materials with tailorable sizes.

1. Introduction

Since the discovery of MCM-41 by Mobil scientists in 1992,[1] mesoporous periodic materials have attracted considerable attention for their potential use as versatile catalysts and supports,[2] and numerous new mesophases with a wide range of pore sizes from 1.6 to 30 nm have been synthesized, such as M41S,[1] SBA-15,[3] HMS,[4] and MSU series.[5] The pore sizes of MCM-41 are claimed to vary from 1.6 to 10 nm in the early literature; however, later results show that the pore sizes of MCM-41 are mainly from 2.5 to 6.5 nm synthesized using alkyltrimethylammonium with different alkyl chains as a template.[6−10] The ordered porous materials with a size from 1.5 to 2.5 nm are relatively scarce, but these porous materials are important for shape selectivity in catalysis because most substrates in organic reactions are less than 2.5 nm.[2]

There have been several successful examples for the preparation of ordered porous silica materials with a size of 1.5−2.5 nm.[11−15] For example, Ryoo et al. synthesized ordered mesoporous silica with size varying from 1.96 to 2.61 nm using various double-chain surfactants;[11] Bagshaw et al. showed ordered supermicroporous silica with a size of 1.6−2.0 nm using micelles of quaternary ω-hydroxyalkylammonium salt;[12] Kruk et al. reported ordered porous silica with unprecedented loading of pendant vinyl groups with pore sizes from 1.4 to 2.8 nm;[13] Ying et al. prepared thermal stable ordered mesoporous and microporous zirconium-doped silica with a size from 1.6 to 2.8 nm.[14a]

Recently, commercial block copolymer has been used as a surfactant to synthesize highly ordered mesoporous

* To whom correspondence should be addressed. Fax: +86-431-5168560. E-mail: fsxiao@mail.jlu.edu.cn.

(1) (a) Kresge, C. T.; Leonowicz, M. E.; Roth, W. J.; Vautuli, J. C.; Beck, J. S. *Nature* **1992**, *352*, 710. (b) Beck, J. S.; Vautuli, J. C.; Roth, W. J.; Leonowicz, M. E.; Kresge, C. T.; Schmitt, K. D.; Chu, C. T.-W.; Olson, D. H.; Sheppard, E. W.; Higgins, J. B.; Schlenker, J. L. *J. Am. Chem. Soc.* **1992**, *114*, 10834.

(2) Corma, A. *Chem. Rev*. **1997**, *97*, 2373.

(3) (a) Zhao, D.; Feng, J.; Huo, Q.; Melosh, N.; Fredrickson, G. H.; Chmelka, B. F.; Stucky, G. D. *Science* **1998**, *279*, 548. (b) Zhao, D.; Huo, Q.; Feng, J.; Chmelka, B. F.; Stucky, G. D. *J. Am. Chem. Soc.* **1998**, *120*, 6024.

(4) Tanev, P. T.; Pinnavaia, T. J. *Science* **1995**, *267*, 865.

(5) (a) Bagshaw, S. A.; Prouzet, E.; Pinnavaia, T. J. *Science* **1995**, *269*, 1242. (b) Prouzet, E.; Pinnavaia, T. J. *Angew. Chem., Int. Ed. Engl.* **1997**, *36*, 516.

(6) Khushalani, D.; Kuperman, A.; Ozin, G. A.; Tanaka, K.; Garces, J.; Olken, M. M.; Coombs, N. *Adv. Mater.* **1995**, *7*, 842.

(7) Huo, Q.; Margolese, D. I.; Stucky, G. D. *Chem. Mater.* **1996**, *8*, 1147.

(8) Corma, A.; Kan, Q.; Navarro, M. T.; Perez-Pariente, J.; Rey, F. *Chem. Mater*. **1997**, *9*, 2123.

(9) Kruk, M.; Jaroniec, M.; Sakamoto, Y.; Terasaki, O.; Ryoo, R.; Ko, C. H. *J. Phys. Chem. B* **2000**, *104*, 292.

(10) Sayari, A.; Yang, Y. *J. Phys. Chem. B* **2000**, *104*, 4835.

(11) Ryoo, R.; Park, I.-S.; Jun, S.; Lee, C. W.; Kruk, M.; Jaroniec, M. *J. Am. Chem. Soc.* **2001**, *123*, 1650 and references therein.

(12) (a) Bagshaw, S. A.; Hayman, A. R. *Chem. Commun.* **2000**, 533. (b) Bagshaw, S. A.; Hayman, A. R. *Adv. Mater.* **2001**, *13*, 1011.

(13) Kruk, M.; Asefa, T.; Jaroniec, M.; Ozin, G. A. *J. Am. Chem. Soc.* **2002**, *124*, 6383.

(14) (a) Wong, M. S.; Huang, H. C.; Ying, J. Y. *Chem. Mater.* **2002**, *14*, 1961. (b) Sun, T.; Wong, M. S.; Ying, J. Y. *Chem. Commun.* **2000**, 2057.

(15) (a) Zhao, X. S.; Lu, G. Q.; Hu, X. *Chem. Commun.* **1999**, 1391. (b) Serrano, D. P.; Aguado, J.; Escola, J. M.; Garagorri, E. *Chem. Commun.* **2000**, 2041. (c) Bastardo-Gonzalez, E.; Mokaya, R.; Jones, W. *Chem. Commun.* **2001**, 1016.

10.1021/cm0497475 CCC: $27.50
Published on Web 11/16/2004

silica,[3] and the pore size of mesostructured materials is influenced by crystallization temperature.[3,5b,16] This is explained as the hydrophobicity of PEO in block copolymers increases with temperature, which leads to an increasing of the mesopore size.[3] Therefore, the temperature can be used as an "adjuster" for the pore size in the synthesis of mesoporous materials templated by surfactants containing PEO groups. Notably, although copolymer surfactants are used to synthesize mesoporous materials with various pore sizes,[3,5,16,17] it is difficult to obtain materials with a pore size of less than 2 nm, due to the limitation of hydrocarbon chains (larger than C_8) for copolymer surfactants. If hydrocarbon chains are shorter than C_8 in diblock copolymers, the hydrophobicity of hydrocarbon chains is not enough for formation of the surfactant micelle.

On the other hand, it has been reported that the hydrophobicity of fluorocarbon is much stronger than that of hydrocarbon,[18,19] and this strong hydrophobicity of the short fluorocarbon chain has an advantage for the formation of surfactant micelle with a relatively small diameter.[18] Moreover, the highly thermal and chemical stability of fluorinated surfactants is very useful in the synthesis of pore materials under various conditions including strong acidic, alkaline, or neutral media.[18,19] We demonstrate here that when a semi-fluorinated surfactant with shorter fluorocarbon chains ($CF_3(CF_2)_4(EO)_{10}$, FSO-100) is used as the template, ordered porous silica materials with tailorable pore sizes are successfully synthesized at various crystallization temperatures in both strongly acidic and neutral conditions for the first time. In particular, in some cases the pore sizes of the mesoporous materials are estimated to be less than 2.0 nm by the BJH method. To discuss the results conveniently and clearly, the obtained samples are denoted as JLU-14$_X$ (acidic media) and JLU-15$_X$ (neutral conditions), where X is the crystallization temperature, though the mesostructure of JLU-14 and JLU-15 is very similar.

2. Experimental Section

2.1. Materials. Tetraethyl orthosilicate (TEOS), titanium tetrabutoxide (TBOT), ethanol, hydrochloric acid, hexane, phenol, catechol, hydroquinone, benzoquinone, benzaldehyde, phenylacetaldehyde, styrene, 2,3,6-trimethylphenol, trimethylhydroquinone, trimethylbenzoquinone, ammonia, NH_4F, and H_2O_2 (30%) were purchased from Beijing Chemical Co. $CF_3(CF_2)_4(EO)_{10}$ (FSO-100) and $CF_3(CF_2)_5(EO)_{14}$ (FSN-100) were purchased from DuPont, and tetrapropylammonium hydroxide (TPAOH) and styrene epoxide were purchased from Fluka Chemical Co.

2.2. Synthesis. In a typical synthesis for JLU-14, 0.8 g of FSO-100 was dissolved in 30 mL of H_2O with 3 mL of HCl (10M/L), followed by addition of 1.25 mL of TEOS. After stirring at room temperature for 30 h, the mixture (SiO_2/HCl/FSO/H_2O with a molar ratio of 1/5.6/0.2/314) was transferred into an autoclave for further condensation at various temperatures for 2 days. The products were collected by filtration, dried in air, and calcined at 600 °C for 5 h to remove the semi-fluorinated surfactant template.

In a typical synthesis for JLU-15, 0.8 g of FSO-100 was dissolved in 30 mL of H_2O, followed by addition of 1.25 mL of TEOS. After stirring at room temperature for 48 h, the mixture (SiO_2/FSO/H_2O with a molar ratio of 1/0.2/314) was transferred into an autoclave for further condensation at various temperatures for 3 days. The products were collected by filtration, dried in air, and calcined at 600 °C for 5 h to remove the semi-fluorinated surfactant template.

In a typical synthesis using semi-fluorinated surfactant of FSN-100, 1.1 g of FSN-100 was dissolved in 25 mL of water with 3 mL of HCl (10M/L) and 0.5 mL trimethylbezene, followed by addition of 2 mL of TEOS. After stirring at room temperature for 30 h, the mixture (SiO_2/HCl/FSN/TMB/H_2O with a molar ratio of 1/3.4/0.13/0.5/160) was transferred into an autoclave for further condensation at 100 °C for 2 days. The products were collected by filtration, dried in air, and calcined at 600 °C for 5 h to remove the semi-fluorinated surfactant template.

For the synthesis of Ti−JLU-14, four methods have been employed, including preformed zeolite nanocluster,[20] pH value adjusting,[21] postsynthesis,[22] and direct synthesis.[23]

In a typical synthesis of Ti−JLU-14 assembled from preformed zeolite nanoclusters, 0.8 g of FSO-100 was dissolved in 30 mL of H_2O with 3 mL of HCl, followed by the addition of 6 mL of preformed titanosilicate precursors prepared according to previous literature methods.[20] After stirring at room temperature for 30 h, the mixture (SiO_2/TiO_2/TPAOH/HCl/FSO/H_2O with a molar ratio of 1/0.034/0.27/5.6/0.2/314) was transferred into an autoclave for further condensation at 80 °C for 2 days. The products were collected by filtration, washed with hot ethanol (70 °C) several times to remove surfactants, and dried in air.

In a typical synthesis of Ti−JLU-14 using pH value adjusting,[21] 0.8 g of FSO-100 was dissolved in 30 mL of H_2O with 3 mL of HCl, followed by addition of 1.25 mL of TEOS and a requisite amount of TBOT. After stirring at room temperature for 30 h, the mixture (SiO_2/TiO_2/HCl/FSO/H_2O with a molar ratio of 1/0.034/5.6/0.2/314) was transferred into an autoclave for further condensation at 80 °C for 2 days. When cooled to room temperature, the system was adjusted to neutral (pH $\approx$ 7.5) by adding the requisite amount of $NH_3 \cdot H_2O$. The adjusted mixture was hydrothermally treated at 80 °C for another 48 h. The product was collected by filtration, washed with hot ethanol (70 °C) several times to remove surfactants, and dried in air.

In a typical synthesis of Ti−JLU-14 using postsynthesis,[22] 0.5 g of JLU-14 was dispersed into 50 mL of dry hexane, followed by addition of the requisite amount of TBOT. The mixture (SiO_2/TiO_2 with a molar ratio of 1/0.034) was stirred at room temperature for 12 h and then filtered, dried, and calcined at 400 °C for 4 h in O_2.

In a typical synthesis of Ti−JLU-14 using direct synthesis, 0.8 g of FSO-100 was dissolved in 30 mL of dilute HCl solution (pH = 2) containing a small amount of NH_4F,[23] followed by addition of 1.25 mL of TEOS and the requisite amount of TBOT. Then the mixture (SiO_2/TiO_2/HCl/FSO/H_2O with a molar ratio of 1/0.034/5.6/0.2/314) was transferred into an autoclave for further condensation at 80 °C for 2 days. The

(16) Miyazawa, K.; Inagaki, S. *Chem. Commun.* **2000**, 2121.
(17) Smarsly, B.; Polarz, S.; Antonietti, M. *J. Phys. Chem. B* **2001**, *105*, 10473.
(18) Muto, Y.; Esumi, K.; Meguro, K.; Zana, R. *J. Colloid Interface Sci.* **1987**, *120*, 162.
(19) Han, Y.; Li, D.; Zhao, L.; Song, J.; Yang, X.; Li, N.; Di, Y.; Li, C.; Wu, S.; Xu, X.; Meng, X.; Lin, K.; Xiao, F.-S. *Angew. Chem., Int. Ed.* **2003**, *42*, 3633.
(20) (a) Xiao, F.-S.; Han, Y.; Meng, X.; Yu, Y.; Yang, M.; Wu, S. *J. Am. Chem. Soc.* **2002**, *124*, 888. (b) Han, Y.; Xiao, F.-S.; Wu, S.; Sun, Y.; Meng, X.; Li, D.; Lin, S. *J. Phys. Chem. B* **2001**, *105*, 7963. (c) Meng, X.; Li, D.; Yang, X.; Yu, Y.; Wu, S.; Han, Y.; Yang, Q.; Jiang, D.; Xiao, F.-S. *J. Phys. Chem. B* **2003**, *107*, 8972.
(21) Wu, S.; Han, Y.; Zou, Y.; Song, J.; Zhao, L.; Di, Y.; Liu, S.; Xiao, F.-S. *Chem. Mater.* **2004**, *16*, 486.
(22) (a) Morey, M. S.; O'Brian, S.; Schwarz, S.; Stucky, G. D. *Chem. Mater.* **2000**, *12*, 898. (b) Luan, Z.; Hartmann, M.; Zhao, D.; Zhou, W.; Kevan, L. *Chem. Mater.* **1999**, *11*, 1621. (c) Luan, Z.; Maes, E. M.; van der Heide, P. A. W.; Zhao, D.; Czernuszewicz, R. S.; Keven, L. *Chem. Mater.* **1999**, *11*, 3680.
(23) Zhang, W.; Lu, J.; Han, B.; Li, M.; Xiu, J.; Ying, P.; Li, C. *Chem. Mater.* **2002**, *14*, 3413.

products were collected by filtration, washed with hot ethanol (70 °C) several times to remove surfactants, and dried in air.

MCM-41, SBA-15, and TS-1 samples in this paper were synthesized according to published literature methods,[3,7,24] respectively.

2.3. Characterization. X-ray diffraction patterns (XRD) were obtained with a Siemens D5005 diffractometer using Cu Kα radiation. Transmission electron microscopy (TEM) experiments were performed on a JEM-3010F electron microscope (JEOL, Japan) with an acceleration voltage of 300 kV. The nitrogen isotherms at the temperature of liquid nitrogen were measured using a Micromeritics ASAP 2010M system. The samples were outgassed for 10 h at 300 °C before the measurements. The sample compositions were determined by inductively coupled plasma (ICP) with a Perkin-Elmer plasma 40 emission spectrometer. Infrared (IR) spectra of molecular oxygen or organic substrates adsorbed on the samples were recorded on a FT-IR spectrometer (PE 430) with a resolution of 1 cm^{-1}. Diffuse reflectance ultraviolet−visible (UV−vis) spectra were measured with a PE Lambda 20 spectrometer, and $BaSO_4$ was the internal standard sample. A Perkin-Elmer TGA 7 unit was used to carry out the thermogravimetric analysis (TGA) in air at a heating rate of 20 °C/min.

2.4. Mechanical Stability. Mechanical tests were performed by pelletizing the powder of the sample into a die with a diameter of 12.7 mm using a hand-operated press for 10 min.

2.5. Catalytic Tests. Catalytic experiments were run in a 50 mL glass reactor and stirred with a magnetic stirrer. In a standard run, reactant, catalyst, and solvent were mixed, followed by addition of H_2O_2. After the reactions were over, the products are analyzed by gas chromatography (GC-9A and GC-17A, Shimadzu, using a flame ionization detector) with a flexible quartz capillary column coated with OV-17 or OV-1.

3. Results and Discussions

3.1. Ordered Mesoporous Silica. *XRD.* Figure 1A shows the small-angle X-ray diffraction (XRD) patterns of calcined JLU-14 samples synthesized at various crystallization temperatures under strongly acidic media in the presence of a semi-fluorinated surfactant of FSO-100. Notably, JLU-14_{100} shows four well-resolved peaks at 1.8°, 3.1°, 3.6°, and 4.1° that can be indexed as (100), (110), (200), and (210) reflections associated with the *p6mm* hexagonal symmetry, analogous to MCM-41 and SBA-15.[1,3] The (100) peak reflects a *d* spacing of 4.8 nm (a_0 = 5.5 nm). Interestingly, when the crystallization temperature is reduced from 100 °C to room temperature, the (100) peak is gradually shifted to higher angles, indicating reduction of the *d* spacing value of hexagonal mesostructures (Table 1). For example, JLU-14_{80} and JLU-14_{RT} exhibit a *d* value of 4.7 and 3.9 nm, respectively. Furthermore, we find that the order of JLU-14 mesostructure is strongly influenced by the crystallization temperature. For example, JLU-14_{100} and JLU-14_{80} show four distinct diffraction peaks, JLU-14_{60} shows three peaks, whereas JLU-14_{RT} shows only one peak.

Figure 1B shows XRD patterns of calcined JLU-15 samples synthesized at various crystallization temperatures under neutral conditions in the presence of a semi-fluorinated surfactant of FSO-100. Notably, JLU-15_{100} shows three peaks indexed as (100), (110), and (200) reflections associated with the *p6mm* hexagonal symmetry.[1,3] When decreasing the crystallization temperature from 100 °C to room temperature the *d* spacing value and order of mesostructures also change. Interestingly, although the ordered mesoporous silica materials (JLU-15) are successfully prepared from assembly of

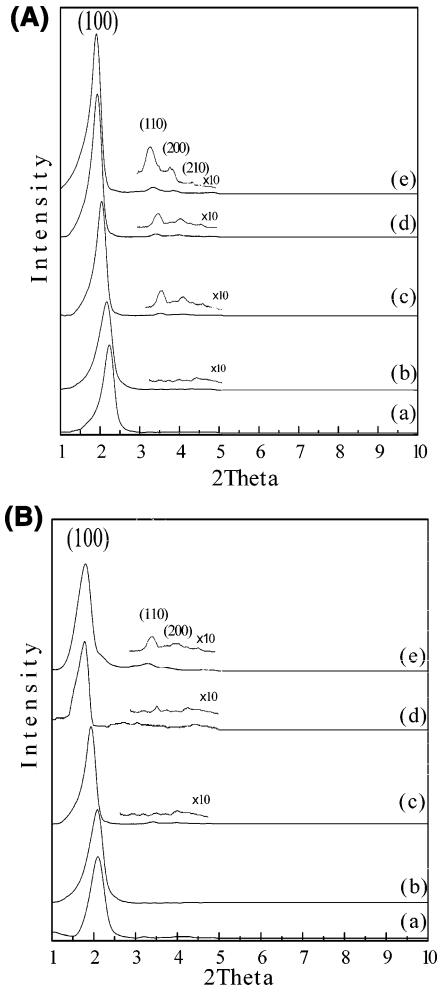

Figure 1. (A) XRD patterns of calcined JLU-14 samples synthesized at various temperatures of (a) JLU-14_{RT}, (b) JLU-14_{40}, (c) JLU-14_{60}, (d) JLU-14_{80}, and (e) JLU-14_{100}; (B) XRD patterns of calcined JLU-15 samples synthesized at various temperatures of (a) JLU-15_{RT}, (b) JLU-15_{40}, (c) JLU-15_{60}, (d) JLU-15_{80}, and (e) JLU-15_{100}.

Table 1. Structure Parameters of the Samples Derived from Nitrogen Adsorption

sample	*d* (nm)	a_0 (nm)	average pore size (nm)	average wall thickness (nm)[a]	surface area (m^2/g)	pore volume (cm^3/g)	*wS/V*
JLU-14_{RT}	3.9	4.5	1.6	2.9	1012	0.51	3.2
JLU-14_{40}	4.0	4.6	1.8	2.8	1106	0.69	2.8
JLU-14_{60}	4.5	5.2	2.3	2.9	1155	0.87	3.1
JLU-14_{80}	4.7	5.4	2.6	2.8	1251	1.01	3.2
JLU-14_{100}	4.8	5.5	3.0	2.5	785	1.05	2.2
JLU-14_{100}[b]	4.9	5.7	3.8	1.9	615	1.12	2.0
JLU-15_{RT}	4.0	4.6	2.0	2.6	1396	0.93	3.0
JLU-15_{40}	4.4	5.1	2.2	2.9	1421	1.12	2.8
JLU-15_{60}	4.9	5.7	2.6	3.1	1500	1.39	2.8
JLU-15_{80}	5.2	6.0	3.4	2.6	1459	1.65	3.0
JLU-15_{100}	5.4	6.2	4.0	2.2	836	1.67	2.0
JLU-15_{100}[b]	5.5	6.4	4.8	1.6	627	1.69	1.8
SBA-15	9.4	10.8	7.2	3.6	870	1.05	6.0
SBA-15[b]	9.5	11	7.9	3.1	700	1.08	5.1
MCM-41	3.6	4.1	2.9	1.2	1080	0.74	4.2
MCM-41[b]					110		

[a] Pore size is calculated from the difference a_0 − pore size. [b] Samples are treated in boiling water for 48 h.

(24) (a) Taramasso, M.; Perego, G.; Notari, B. U.S. Patent 4410501, 1983. (b) Kumar, S.; Mirajkar, S.; Paris, G.; Kumar, P.; Kumar, R. *J. Catal.* **1995**, *156*, 163.

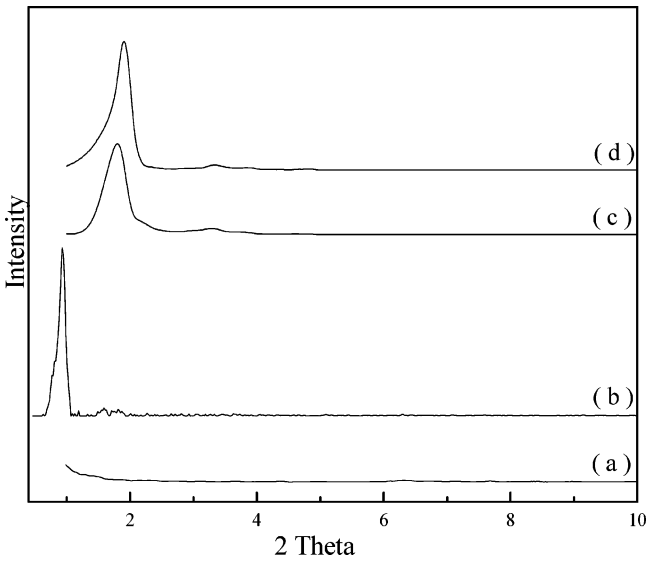

Figure 2. XRD patterns of (a) MCM-41, (b) SBA-15, (c) JLU-15_{100}, and (d) JLU-14_{100} samples treated in boiling water for 48 h.

TEOS with semi-fluorinated surfactants in neutral conditions, they cannot be formed by assembly of TEOS with hydrocarbon surfactants such as copolymer surfactant (Brij 56, $C_{16}EO_{10}$) at the same pH value. Obviously, the semi-fluorinated surfactant plays an important role for the formation of ordered mesostructures under neutral conditions. Generally, mesostructured materials synthesized in neutral conditions are wormlike,[5] except for MSU-H assembled from water-soluble silicates.[25]

XRD patterns of as-synthesized samples (Supporting Information, Figure 1) are very similar to those of calcined samples, except that the peaks slightly shift to low angles, indicating contraction of the unit cell during calcination.

Thermogravimetric analyses (TGA) of as-synthesized JLU-14_{100} sample (Supporting Information Figure 2) show that there is a total weight loss of 52%. The initial weight loss below 373 K is mainly assigned to removal of adsorbed water (<5%), and about 40% weight loss occurs from 463 to 573 K, due to decomposition of ethylene oxide (EO) section, and followed by 8% weight loss at higher temperatures (573−723 K) due to the decomposition of fluorinated carbon.

Figure 2 shows XRD patterns of MCM-41, SBA-15, JLU-14_{100}, and JLU-15_{100} treated in boiling water for 48 h. It is well known that SBA-15 samples have much better hydrothermal stability than MCM-41. After treatment of SBA-15 for 48 h, SBA-15 still exhibits its XRD peaks associated with hexagonal mesopores, in good agreement with those reported by Zhao et al.[3] Interestingly, both JLU-14_{100} and JLU-15_{100} also show similar hydrothermal stability with SBA-15. After hydrothermal treatment in boiling water for 48 h, both JLU-14_{100} and JLU-15_{100} still retain their mesostructures, giving typical peaks associated with hexagonal mesopores which can be indexed as (100), (110), and (200). In contrast, the same hydrothermal treatment leads to complete destruction of MCM-41 mesostructure. Apparently, both JLU-14_{100} and JLU-15_{100} have better hydrothermal stability than MCM-41.

As observed in Figures 1 and 2, it is obvious that the peak of JLU-14_{100} and JLU-15_{100} is much wider than that of SBA-15, although all of these materials have hexagonal symmetry. For example, the semi-peak width of JLU-14_{100} and JLU-15_{100} is at 0.31° and 0.39°, respectively. In contrast, SBA-15 gives a semi-peak width at 0.11°. Generally, semi-peak width is strongly related to the ordering and uniformity of mesostructures.[26]

Figure 3 shows XRD patterns of JLU-14_{100}, JLU-15_{100}, and SBA-15 samples under a pressure range of 0−700 MPa for 10 min. It has been reported that MCM-41 and SBA-15 completely lose XRD peaks if the pelletizing pressure is higher than 450 MPa, due to decay of the mesostructure.[27b] However, under similar pressure (385 MPa), JLU-14_{100} and JLU-15_{100} samples still retain partial XRD peaks associated with mesostructure (Figure 3A and B), indicating their high mechanical stability. Even when the pressure is increased to 700 MPa, JLU-14_{100} and JLU-15_{100} also show one peak (Figure 3A and B). On the contrary, SBA-15 shows only a very weak peak under the pressure at 385 MPa, and XRD patterns of SBA-15 completely disappear when the pressure reaches 700 MPa (Figure 3C). All of these results indicate that JLU-14 and JLU-15 have much a higher mechanical stability than SBA-15, which is potentially important for industrial applications such as preparation of samples and catalytic reactions under high pressure.[27]

The higher mechanical stability of JLU-14 and JLU-15 could be attributed to the larger ratio of wall thickness (t) to cell parameter (a_0). It has been reported that the elasticity limit of hexagonal honeycomb materials is controlled by the square of the ratio for wall thickness to cell parameters $[(t/a_0)^2]$.[27d] The ratio of wall thickness to cell parameters for JLU-14_{100} and JLU-15_{100} samples is 0.455 and 0.354, respectively, which is obviously larger than that of MCM-41 (0.293) and SBA-15 (0.331).

TEM. Figure 4 shows transmission electron micrograph (TEM) images of various samples. Obviously, the pores of these samples are ordered hexagonal-like. From high-dark contrast in the TEM image of the sample the distance between mesopores is estimated. Clearly, the distance between pores for the samples synthesized at 80 °C (JLU-14_{80} and JLU-15_{80}) is much larger than that for the samples synthesized at room temperature (JLU-14_{RT} and JLU-15_{RT}), in a good agreement with the value measured with XRD. For example, the distance between mesopores for JLU-14_{80} and JLU-14_{RT} is estimated to be 55 and 42 Å, which is close to that determined from XRD (JLU-14_{80} and JLU-14_{RT} at 54 and 44 Å, respectively).

(25) (a) Kim, S.-S.; Pauly, T. R.; Pinnavaia, T. J. *Chem. Commun.* **2000**, 1661. (b) Kim, S.-S.; Karkamkar, A.; Pinnavaia, T. J.; Kruk, M.; Jaroniec, M. *J. Phys. Chem. B* **2001**, *105*, 7663.

(26) Han, Y.; Wu, S.; Sun, Y.; Li, D.; Xiao, F.-S. *Chem. Mater.* **2002**, *14*, 1144.

(27) (a) Gusev, Y. V.; Feng, X.; Bu, Z.; Haller, G. L.; O'Brian, J. A. *J. Phys. Chem.* **1996**, *100*, 1985. (b) Cassiers, K.; Linssen, T.; Mathieu, M.; Benjelloun, M.; Schrijnemakers, K.; van der Voort, P.; Cool, P.; Vansant, E. F. *Chem. Mater.* **2002**, *14*, 2317. (c) Hartmann, M.; Vinu, A. *Langmuir* **2002**, *18*, 8010. (d) Galarneau, A.; Desplantier-Giscard, D.; Di Renzo, F.; Fajula, F. *Catal. Today* **2001**, *68*, 191 and references therein.

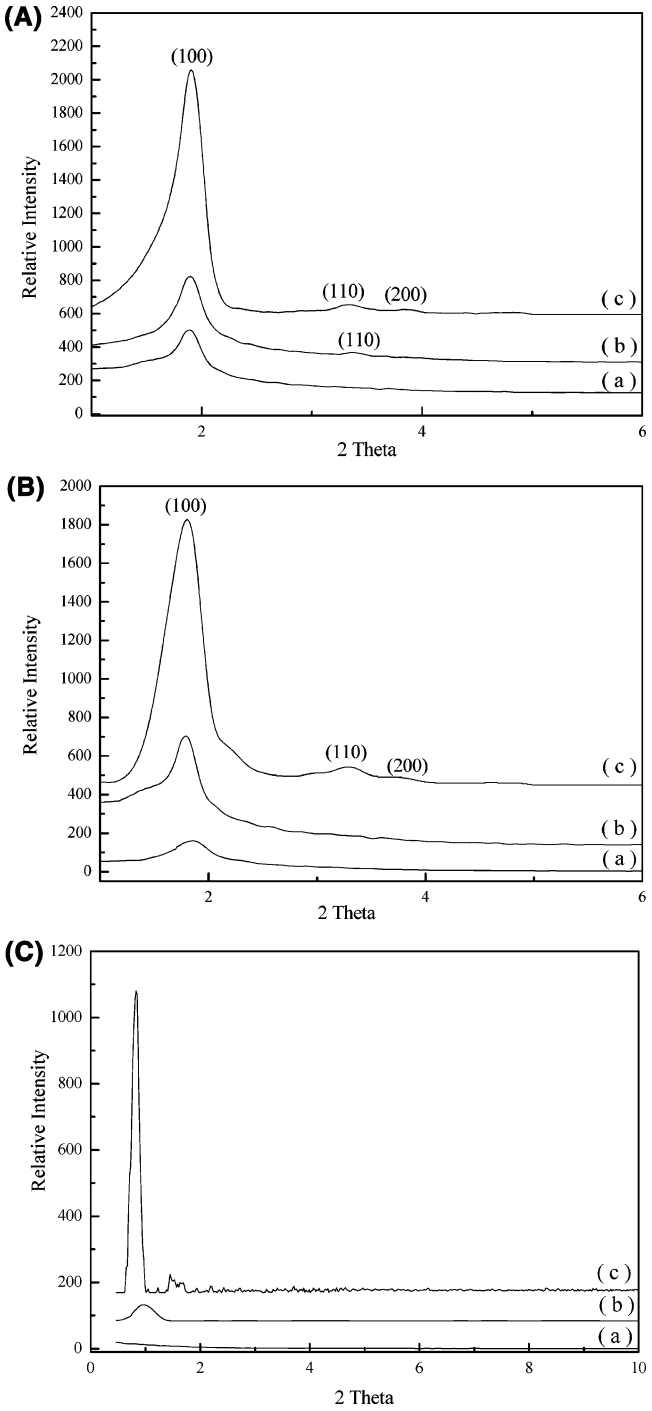

Figure 3. XRD patterns of (A) JLU-14_{100}, (B) JLU-15_{100}, and (C) SBA-15 samples under a pressure of (a) 700 MPa, (b) 385 MPa for 10 min, and (c) under the atmosphere.

Interestingly, as observed in Figure 4, the wall thickness of JLU-14_{80} and JLU-15_{80} is about 2.5 nm, which is greater than that of MCM-41 reported in the literature.[1,2] The thicker mesoporous walls of JLU-14 and JLU-15 may be responsible for the higher hydrothermal and mechanical stability than that of MCM-41.

Furthermore, we found that the pore size of various samples is obviously distinguishable (Figure 4). For example, the pore size of JLU-14_{80} is estimated at ~3 nm, while the pore size of JLU-14_{RT} is estimated at ~1.7 nm. Therefore, the pore size of JLU-14 and JLU-15

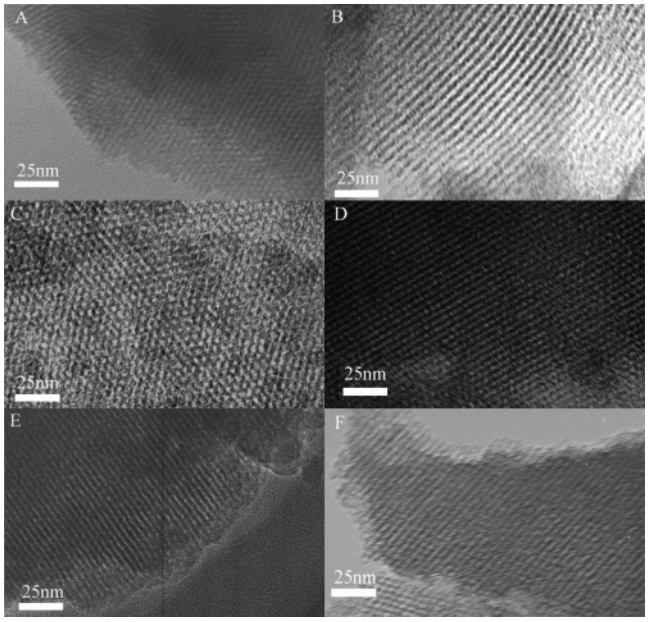

Figure 4. Transmission electron microscopy (TEM) images of JLU-14_{80} taken in (A) [100] and (B) [110] directions, JLU-15_{80} taken in (C) [100] and (D) [110] directions, JLU-14_{RT} taken in the [110] direction (E), and JLU-15_{RT} taken in the [110] direction (F).

could be tailored by changing the synthetic crystallization temperature.

N_2 Isotherms. Figure 5 shows N_2 isotherms for JLU-14 and JLU-15, and the parameters are summarized in Table 1. Generally, all of N_2 isotherms for various samples basically show IV-type curves. However, as the crystallization temperature decreased from 100 °C to room temperature, capillary condensation takes place at lower relative pressure. For example, JLU-14_{RT} and JLU-14_{40} display a well-defined capillary condensation step at relative pressures (P/P_0) of 0.09−0.13 and 0.12−0.16, respectively, indicating formation of small pores with diameters less than 2.0 nm. Similar phenomena have been observed in the isotherms of M41S, SBA-8, and IROU-1.[14,28] Correspondingly, pore sizes for JLU-14_{RT} and JLU-14_{40} were calculated using the BJH method, which produced values centered around 1.6 and 1.8 nm (Table 1). Various researchers have debated the reliability of this model,[29] but it appears to be generally valid in the size range under consideration here. In contrast, the isotherms of JLU-14_{80} and JLU-14_{60} show a hysteresis loop at a relative pressure of 0.3−0.45, characteristic of mesopores. Estimation of pore sizes by the BJH method gives values at 2.6 and 2.3 nm for JLU-14_{80} and JLU-14_{60}, respectively. Considering these isotherms of various samples, it is very interesting to note that the pore sizes are obviously changed from micropore to mesopore by assembly of semi-fluorinated surfactant (FSO-100) with silica species at various crystallization temperatures, i.e., a pore size in the region of 1.6−4.0 nm could be tailored by the choice of crystallization temperature for the synthesis of JLU-

(28) (a) Kruk, M.; Jaroniec, M.; Sayari, A. *J. Phys. Chem. B* **1997**, *101*, 583. (b) Zhao, D.; Huo, Q.; Feng, J.; Kim, J.; Han, Y.; Stucky, G. D. *Chem. Mater.* **1999**, *11*, 2668.

(29) (a) Galarneau, A.; Desplantier, D.; Dutartre, R.; Renzo, F. Di *Micro. Meso. Mater.* **1999**, *27*, 297. (b) Lukns, W. W.; Schmidt-Winkel, P.; Zhao, D.; Feng, J.; Stucky, G. D. *Langmuir* **1999**, *15*, 5403.

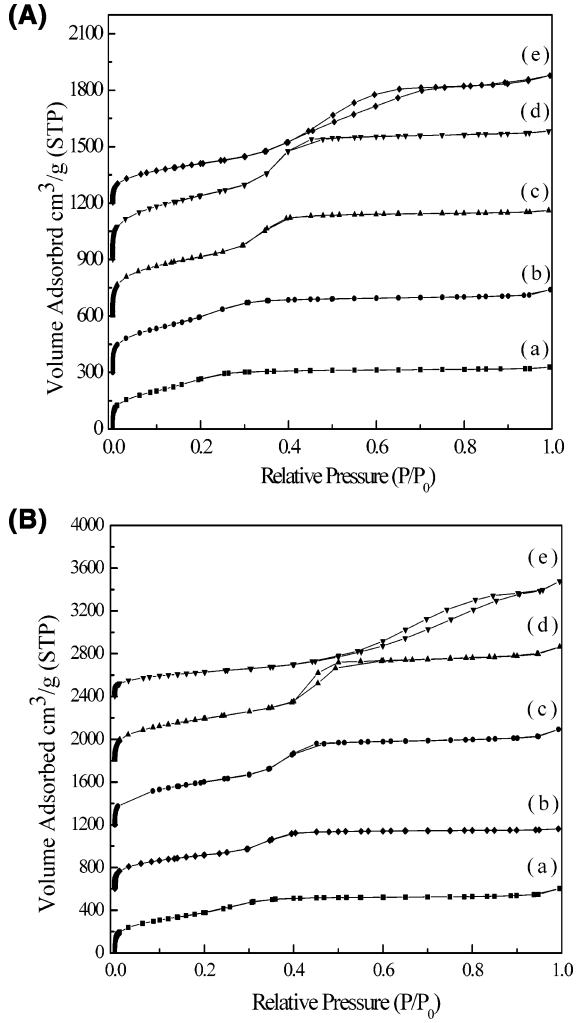

Figure 5. (A) Nitrogen isotherms of JLU-14 samples synthesized at various temperatures of (a) JLU-14_{RT}, (b) JLU-14_{40}, (c) JLU-14_{60}, (d) JLU-14_{80}, and (e) JLU-14_{100}. The isotherms for JLU-14_{40}, JLU-14_{60}, JLU-14_{80}, and JLU-14_{100} are offset from 300, 600, 900, and 1200 cm^3/g to begin with for clarity, respectively. (B) Nitrogen isotherms of JLU-15 samples synthesized at various temperatures of (a) JLU-15_{RT}, (b) JLU-15_{40}, (c) JLU-15_{60}, (d) JLU-15_{80}, and (e) JLU-15_{100}. The isotherms for JLU-15_{40}, JLU-15_{60}, JLU-15_{80}, and JLU-15_{100}, are offset from 600, 1200, 1800, and 2400 cm^3/g to begin with for clarity, respectively.

14 and JLU-15. The ordered micropores in JLU-14 and JLU-15 are reasonably assigned to a relatively small micelle of semi-fluorinated surfactant with a short fluorocarbon chain (FSO-100). To the best of our knowledge, this is the first time ordered porous silica materials with a pore size less than 2.0 nm has been prepared using nonionic polymer surfactants, although ordered microporous silica materials with a pore size of 1.5−2.5 nm have been synthesized using ammonium surfactants.[15]

Furthermore, nitrogen isotherms also estimate that mesoporous walls of JLU-14 and JLU-15 are much thicker than that of MCM-41, which is responsible for the higher hydrothermal stability of JLU-14 and JLU-15 than that of MCM-41.

It is interesting to note that JLU-14 and JLU-15 have a relatively large surface area when compared with SBA-15, e.g., JLU-15_{60} gives rise to a BET surface area of 1500 m^2/g, which is much higher than that of SBA-15 (700−1000 m^2/g) and MCM-41 (800−1300 m^2/g).[1−3,7,15] The larger surface area of porous materials is very important for the preparation of catalysts or catalyst supports with higher activity in industrial application.[2]

One possibility of JLU-15 with a large surface area is due to the presence of micropores in mesoporous walls. Generally, microporosity in mesoporous materials is measured with *t* plots. If *t* plots of mesoporous materials do not pass zero of the axis, it means that there are micropores in the mesoporous materials. Inagaki et al. reported that there are some micropores in the walls of SBA-15 formed by penetration of hydrophilic poly(ethylene oxide) chains of triblock copolymer in the silica wall.[30] The *t* plot of JLU-15_{60} (Supporting Information Figure 3) shows that the *t* plot passes zero of the axis, meaning there are no micropores in them.

Another possibility of JLU-15 with a large surface area is attributed to the fact that hexagonal mesopores in JLU-15 are not simple cylinders. Ryoo and Jaroniec et al. investigated the relationship between the structural parameters for materials with uniform pores.[31] If wS/V (w, S, and V denote pore size, surface area, and pore volume, respectively) is close to 4, the mesopores model should be simply cylindrical geometry.[31] In fact, the obtained values of wS/V for most JLU-14 and JLU-15 samples are at 2.8−3.2 (Table 1), indicating that the mesopores are not simply of cylindrical geometry, although XRD and TEM have confirmed the hexagonal mesopores. Possibly the channels of mesopores may be like pearl bunches. Further study for their mesostructures is under investigation.

Kim and Stucky et al. carefully investigated the relationship between the hydrophilic−hydrophobic balance of the amphiphilic block copolymers with the mesostructure of the mesoporous silica.[32] Generally, the molar volume of hydrophilic headgroups can be calculated by the sum of molar volumes of poly(ethylene oxide) and hydroxide: $V_H = xV_{EO} + V_{OH}$, where V_H, V_{EO}, and V_{OH} are the molar volumes of the hydrophilic part, the total ethylene oxide (EO) group, and the hydroxyl group, respectively, and x is the number of EO units.[32,33] The volume of the hydrophobic part (V_L) can be obtained by $V_L = nV_C$, where n is the number of carbon units and V_C is the molar volume of a carbon unit.[32,33] They reported that values V_H/V_L at 1.0−1.7 result in formation of 2D hexagonal mesostructures.[32] Similarly, we also calculated V_H/V_L of semi-fluorinated surfactants, and the obtained value is 1.6, which is in good agreement with the range of 2D hexagonal mesostructure.[32]

As discussed above, obvious features for semi-fluorinated surfactant syntheses of ordered mesoporous silica materials are as follows: (1) tailorable pore size from 1.6 to 4.0 nm, estimated by BJH and TEM methods; (2) the pH value for a synthetic system is extended to neutral conditions; (3) thicker porous walls, showing high hydrothermal and mechanical stability; in particular, these materials, such as JLU-14, exhibit much

(30) Miyazawa, K.; Inagaki, S. *Chem. Commun*. **2000**, 2121.
(31) Ryoo, R.; Ko, C. H.; Kruk, M.; Antochshuk, V.; Jaroniec, M. *J. Phys. Chem. B* **2000**, *104*, 11465.
(32) Kim, J. M.; Sakamoto, Y.; Hwang, Y. K.; Kwon, Y.-U.; Terasaki, O.; Park, S.-E.; Stucky, G. D. *J. Phys. Chem. B* **2002**, *106*, 2552.
(33) Kunieda, H.; Shigeta, K.; Ozawa, K.; Suzuki, M. *J. Phys. Chem. B* **1997**, *101*, 7952.

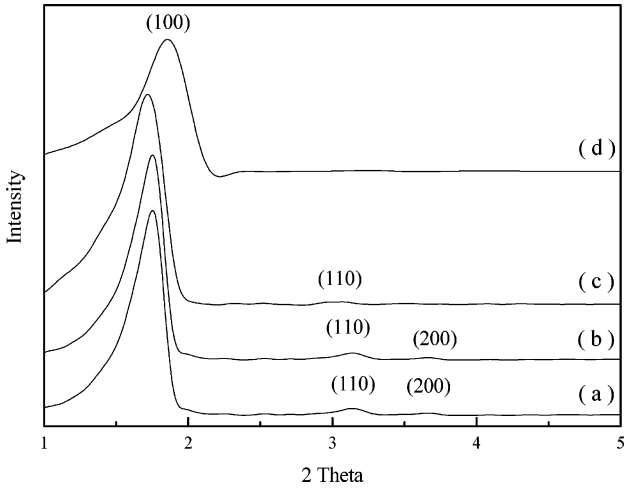

Figure 6. XRD patterns of Ti−JLU-14_{80} synthesized from (a) preformed titanosilicate nanoclusters, (b) pH value adjusting, (c) direct synthesis, and (d) postsynthesis.

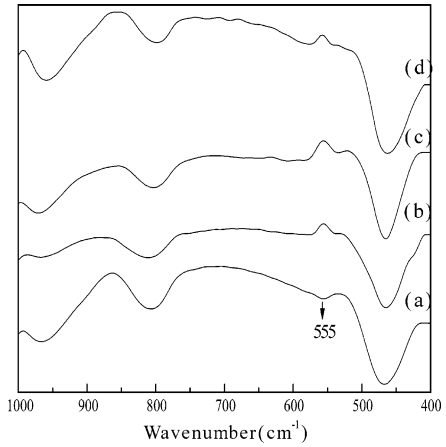

Figure 7. IR spectra of Ti−JLU-14_{80} synthesized from (a) preformed titanosilicate nanoclusters, (b) pH value adjusting, (c) direct synthesis, and (d) postsynthesis.

higher mechanical stability than SBA-15 and MCM-41; (4) very large surface area, for example, the surface area of JLU-15_{60} is as high as 1500 m^2/g.

It is worth noting that semi-fluorinated surfactant synthesis is not limited to the use of FSO-100, and many semi-fluorinated surfactants can be used if they effectively form a regular micelle in solution. For example, when semi-fluorinated surfactant of $CF_3(CF_2)_5(EO)_{14}$ (FSN-100) is used as a template, ordered hexagonal-like mesoporous silica materials with a pore size of 2.0−5.0 nm have been successfully synthesized in strongly acidic media. The XRD pattern in Supporting Information Figure 4 shows hexagonal-like mesoporous silica materials synthesized at 100 °C using FSN-100 as a template. Possibly, semi-fluorocarbon surfactant synthesis is a novel way to prepare a series of ordered mesoporous materials with tailorable size from micropore to mesopore.[32]

3.2. Incorporation of Heteroatoms into Ordered Mesoporous Silica. Heterogeneous atoms of Al- and Ti−substituted materials, with the goal of introducing catalytically active sites, have been successfully synthesized by direct synthesis,[23] postsynthesis,[22] pH value adjusting,[21] and preformed zeolite nanoclusters.[20,34] As an example, here we show synthesis, characterization, and catalysis of ordered mesoporous titanosilicate (Ti−JLU-14_{80}).

The samples are denoted as Ti−JLU-14(*y*), where *y* stands for direct synthesis (d), postsynthesis (p), pH value adjusting (a), and nanoclusters (n), respectively.

XRD. Figure 6 shows the small-angle XRD patterns of Ti−JLU-14 samples synthesized by various routes. Ti−JLU-14(n) and Ti−JLU-14(a) samples both clearly show three peaks indexed as (100), (110), and (200) assigned to hexagonal mesopores, and Ti−JLU-14(d) shows two peaks, while Ti−JLU-14(p) shows only one peak. Apparently introduction of Ti into the mesoporous silica leads to a decrease of the order of mesostructure,[2] but the various routes are distinguishable for the mesostructured order. Ti−JLU-14(n) exhibits three XRD peaks, indicating a good order of mesostructure, while Ti−JLU-14(p) shows only one XRD peak, indicating very low order of mesostructure. Furthermore, we observed that the *d* spacings of (100) in Ti−JLU-14(d), Ti−JLU-14(n), and Ti−JLU-14(a) are at ∼5.1 nm, which is obviously larger than that in JLU-14. Furthermore, no diffraction peak is observed in the higher angle region 10−40° for Ti−JLU-14(n) (Supporting Information Figure 5), which indicates the absence of large microporous crystals in the sample, suggesting that Ti−JLU-14(n) sample is a pure phase.

IR Spectroscopy. Figure 7 gives IR spectra of various Ti−JLU-14 samples. IR spectra of Ti−JLU-14(p), Ti−JLU-14(d), and Ti−JLU-14(a) samples only show a broad band at 460 cm^{-1} in the region of 400−600 cm^{-1}, which is similar to that of amorphous titanosilicate materials. However, Ti−JLU-14(n) exhibits an obvious band at 555 cm^{-1} in addition to the band at 460 cm^{-1}. The band at ∼555 cm^{-1} is similar to that of five-membered rings of T−O−T (T = Si or Al) in microporous zeolites.[35] This result suggests that Ti−JLU-14(n) has zeolite primary and secondary building units.[20]

UV−Vis Spectroscopy. UV−vis spectroscopy is a very common method for characterization of the coordination number of Ti species in the zeolite framework.[2,20,36] Figure 8 shows the spectra of various Ti−JLU-14. Ti−JLU-14(n) has an obvious adsorption band at 218 nm, which is the same as that of TS-1, assigned to the titanium species in T_d coordination. The absence of a band at 330 nm implies that anatase phase is not present, due to the strongly acidic conditions preventing the formation of TiO_2. In contrast, the UV−vis spectra of the other three Ti−JLU-14 samples prepared from direct synthesis, postsynthesis, and pH value adjusting show a much broader adsorption band centered at 230−

(34) (a) Zhang, Z.; Han, Y.; Zhu, L.; Wang, R.; Yu, Y.; Qiu, S.; Zhao, D.; Xiao, F.-S. *Angew. Chem., Int. Ed.* **2001**, *40*, 1258. (b) Liu, Y.; Zhang, W.; Pinnavaia, T. J. *Angew. Chem., Int. Ed.* **2001**, *40*, 1255.

(35) (a) Breck, D. W. *Zeolite Molecular Sieves*; Wiely: New York, 1974. (b) Jacobs, P. A.; Derouane, E. G.; Weitkamp, J. *J. Chem. Soc., Chem. Commun.* **1981**, 591.

(36) (a) Zecchina, A.; Spoto, G.; Bordiga, S.; Ferrero, A.; Petrini, G.; Padovan, M.; Leofanti, G. *Stud. Surf. Sci. Catal.* **1991**, *69*, 251. (b) Ricchiardi, G.; Damin, A.; Bordiga, S.; Lamberti, C.; Spanò, G.; Rivetti, F.; Zecchina, A. *J. Am. Chem. Soc.* **2001**, *121*, 11409. (c) Bordiga, S.; Coluccia, S.; Lamberti, C.; Marchese, L.; Zecchina, A.; Boscherini, F.; Buffa, F.; Genoni, F.; Leofanti, G.; Petrini, G.; Vlaic, G. *J. Phys. Chem.* **1994**, *98*, 4125. (d) Lamberti, C.; Bordiga, S.; Arduino, D.; Zecchina, A.; Geobaldo, F.; Spanò, G.; Genoni, F.; Petrini, G.; Carati, A.; Villain, F.; Vlaic, G. *J. Phys. Chem. B* **1998**, *102*, 6382. (e) Zecchina, A.; Bordiga, S.; Lamberti, C.; Ricchiardi, G.; Scarano, D.; Petrini, G.; Leofanti, G.; Mantegazza, M. *Catal. Today* **1996**, *32*, 97.

Table 2. Catalytic Activities in Oxidations by H_2O_2 over Various Ti−JLU-14_{80} Catalysts

catalyst	reaction	conversion (%)	product selectivity (%)		
			P1	P2	P3
Ti−JLU-14(n)	phenol hydroxylation[a]	23.2	58.1	39.9	2.0
Ti−JLU-14(a)	phenol hydroxylation[a]	2.2	58.4	39.2	2.4
Ti−JLU-14(p)	phenol hydroxylation[a]	1.7	57.5	39.5	3.0
Ti−JLU-14(d)	phenol hydroxylation[a]	2.1	56.3	40.1	3.6
Ti−JLU-14(n)	styrene epoxidation[b]	12.1	35.7	8.2	56.1
Ti−JLU-14(a)	styrene epoxidation[b]	10.2			100
Ti−JLU-14(p)	styrene epoxidation[b]	8.8			100
Ti−JLU-14(d)	styrene epoxidation[b]	9.3			100
Ti−JLU-14(n)	2,3,6-trimethylphenol hydroxylation[c]	12.6	65.2	21.7	13.1
Ti−JLU-14(a)	2,3,6-trimethylphenol hydroxylation[c]	5.2	64.1	22.4	13.5
Ti−JLU-14(p)	2,3,6-trimethylphenol hydroxylation[c]	3.1	64.7	21.4	13.9
Ti−JLU-14(d)	2,3,6-trimethylphenol hydroxylation[c]	4.9	65.3	22.1	12.6

[a] Reaction conditions: water as a solvent, reaction temperature at 80 °C, phenol/H_2O_2 = 3/1 (molar ratio), reaction time for 4 h, catalyst/phenol = 5% (weight ratio). The products are catechol (P1), hydroquinone (P2), and benzoquinone (P3). The product of tar is not included. [b] Reaction conditions: Acetone as a solvent, reaction temperature at 45 °C, styrene/H_2O_2 = 3/1 (molar ratio), reaction time for 5 h, catalyst/phenol = 5% (weight ratio). The products are styrene epoxide (P1), phenylacetaldehyde (P2), and benzaldehyde (P3). [c] Reaction conditions: Acetonitrile as a solvent, reaction temperature at 80 °C, trimethylphenol/H_2O_2 = 3/1 (molar ratio), reaction time for 4 h, catalyst/phenol = 5% (weight ratio). The products are trimethylhydroquinone (P1), trimethylbenzoquinone (P2), others (P3).

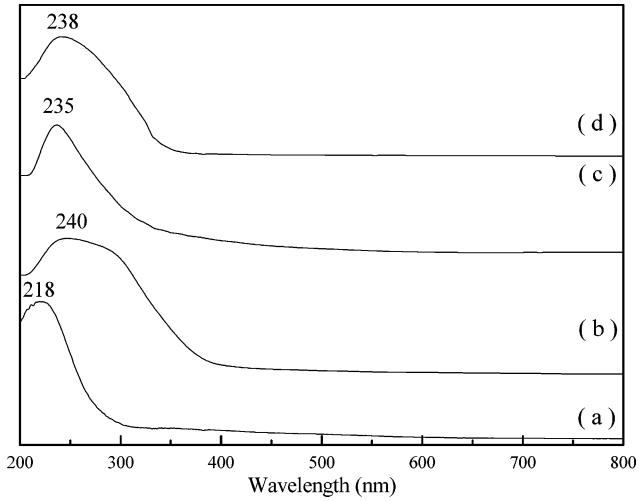

Figure 8. UV−vis spectra of Ti−JLU-14_{80} synthesized from (a) preformed titanosilicate nanoclusters, (b) pH value adjusting, (c) direct synthesis, and (d) postsynthesis.

240 nm, which is assigned to Ti species in the amorphous nature with a coordination number between 4 and 6. These results indicate that the nature of titanium coordination in the Ti−JLU-14(n) sample is distinguishable from that of the other three Ti−JLU-14 samples.

Catalytic Properties. Catalytic data of the oxidation of aromatics by H_2O_2 over various Ti−JLU-14 catalysts are presented in Table 2. ICP results showed that all Ti−JLU-14 samples have a similar titanium content of Si/Ti = 28−34 molar ratio, and no leaching of Ti species was found in the reaction solutions.

In phenol hydroxylation, Ti−JLU-14(n) exhibits excellent activity, giving the conversion at 23.2%, which is comparable the activities of TS-1 and MTS-9 catalysts.[20] On the contrary, the other three titanosilicates prepared from direct synthesis, postsynthesis, and pH value adjusting show relatively low activities, giving conversion at 1.7−2.2%. The big difference between Ti−JLU-14(n) and the other three Ti−JLU-14 samples is reasonably attributed to the difference of titanium species in these mesoporous titanosilicates. The titanium species in Ti−JLU-14(n) is TS-1 like, showing similar oxidation abilities to TS-1 and MTS-9. In contrast, titanium species in the other three Ti−JLU-14 samples are of an amorphous nature in the mesoporous walls, resulting in very low conversion for phenol hydroxylation with hydrogen peroxide, which is similar to that of Ti−MCM-41.[20]

In styrene epoxidation by hydrogen peroxide (Table 2), all samples of Ti−JLU-14 are active but the product selectivity is quite different. Ti−JLU-14(n) show high selectivity for the epoxide products (43.9%), including styrene epoxide and phenylacetaldehyde, which is comparable with that of MTS-9.[20,37] However, the other three titanosilicates show 100% selectivity for benzaldehyde, which is similar to that of Ti−MCM-41. The big difference in product selectivity indicates that the reaction mechanism and route in this reaction between Ti−JLU-14(n) and the other mesoporous titanosilicates is distinguishable, which is assigned to the difference for titanium species in these titanosilicate catalysts.[20]

In the hydroxylation of trimethylphenol (Table 2), Ti−JLU-14(d), Ti−JLU-14(p), and Ti−JLU-14(a) show low conversion at 4.9%, 3.1%, and 5.2%, respectively, which is due to the relatively low oxidation ability of Ti species in the amorphous wall of mesoporous materials. Interestingly, Ti−JLU-14(n) is more active for this reaction with a conversion of 12.6%, indicating that Ti−JLU-14(n) is an effective catalyst for the oxidation of bulky molecules, which is similar to that of MTS-9. However, TS-1 is inactive due to the inaccessibility of the small micropores of TS-1 to the large diameter of trimethylphenol.[20] The high activity in the hydroxylation of trimethylphenol over Ti−JLU-14(n) is also attributed to titanium species like TS-1.

It is not surprising to find that Ti−JLU-14(n) shows a similar catalytic behavior to that of mesoporous titanosilicates of MTS-9 because the same preformed titanosilicates (TS-1) precursors are used to assemble with polymer surfactant (FSO or P123) in the preparation.[20] The difference of these catalysts is the pore size. For example, the pore size of Ti−JLU-14 can be tailorable from microporous to mesoporous (1.6−4 nm), while the pore size of MTS-9 is larger (7−9 nm).

(37) Yang, Q.; Wang, S.; Lu, J.; Xiong, G.; Feng, Z.; Xin, Q.; Li, C. *Appl. Catal. A: Gen.* **2000**, *194*, 507.

4. Conclusions

Novel ordered mesoporous silica-based materials (JLU-14 and JLU-15) with tailorable size from micropore to mesopore (1.6−4.0 nm) are successfully synthesized by changing crystallization temperatures from room temperature to 100 °C in both strongly acidic media and neutral conditions using semi-fluorinated surfactant (FSO-100). JLU-14 and JLU-15 samples show much higher hydrothermal and mechanical stability than MCM-41 due to their relatively thicker walls. Furthermore, titanium species have been effectively introduced into mesoporous silica of JLU-14 by various routes including direct synthesis, postsynthesis, pH value adjusting, and preformed TS-1 zeolite nanoclusters. Catalytic results show that Ti−JLU-14 assembled from preformed TS-1 nanoclusters is very active in both small molecular oxidation (phenol hydroxylation and styrene epoxidation) and bulky molecular oxidation (2,3,6-trimethylphenol hydroxylation). In contrast, the other mesoporous titanosilicates prepared from direct synthesis, postsynthesis, and pH value adjusting exhibit low activities in these catalytic reactions. The difference in catalytic activities among the mesoporous Ti−JLU-14 samples is assigned to the difference of the nature of titanium species in the mesoporous walls. Characterization of these samples shows that Ti species in Ti−JLU-14 assembled from preformed titanosilicate nanoclusters are TS-1 like, while Ti species in the other mesoporous titanosilicates are amorphous in nature, in good agreement with those of Ti−MCM-41.

Acknowledgment. This work is supported by NSFC, CNPC, State Basic Research Project, and National High Technology Research and Development Program of China.

Supporting Information Available: XRD patterns of as-synthesized JLU-14 and JLU-15 at various temperatures, TG curve of JLU-14_{100}, t plots of JLU-15_{60}, and XRD pattern of Ti−JLU-14(n) (pdf). This material is available free of charge via the Internet at http://pubs.acs.org.

CM0497475